Research Square

Preprints are preliminary reports that have not undergone peer review.
They should not be considered conclusive, used to inform clinical practice,
or referenced by the media as validated information.

Basis for drug selectivity of plasmepsin IX and X inhibition for *Plasmodium falciparum* and *vivax*

Anthony N. Hodder
The Walter and Eliza Hall Institute of Medical Research
Janni Christensen1
The Walter and Eliza Hall Institute of Medical Research
Stephen Scally
The Walter and Eliza Hall Institute of Medical Research
Tony Triglia
The Walter and Eliza Hall Institute of Medical Research
Anna Ngo
The Walter and Eliza Hall Institute of Medical Research
Richard W. Birkinshaw
The Walter and Eliza Hall Institute of Medical Research
Brodie Bailey
The Walter and Eliza Hall Institute of Medical Research
Paola Favuzza
The Walter and Eliza Hall Institute of Medical Research
Melanie H. Dietrich
The Walter and Eliza Hall Institute of Medical Research
Wai-Hong Tham
The Walter and Eliza Hall Institute of Medical Research
Peter E. Czabotar
The Walter and Eliza Hall Institute of Medical Research
Kym Lowes
The Walter and Eliza Hall Institute of Medical Research
Zhuyan Guo
Merck & Co., Inc.
Nicholas Murgolo
Merck & Co., Inc.
Manuel de Lera Ruiz
Merck & Co., Inc.
John A. McCauley
Merck & Co., Inc.
Brad E. Sleebs

The Walter and Eliza Hall Institute of Medical Research

David Olsen

Merck & Co., Inc.

Alan F. Cowman (cowman@wehi.edu.au)

The Walter and Eliza Hall Institute of Medical Research https://orcid.org/0000-0001-5145-9004

Research Article

Keywords: malaria, aspartic protease, antimalarial, plasmepsin IX, plasmepsin X

Posted Date: September 29th, 2021

DOI: https://doi.org/10.21203/rs.3.rs-944781/v1

License: This work is licensed under a Creative Commons Attribution 4.0 International License.
Read Full License

Abstract

Plasmepsin IX (PMIX) and X (PMX) are aspartyl proteases of *Plasmodium* spp. that play essential roles in parasite egress, invasion and development. Consequently, they are important drug targets for *Plasmodium falciparum* and *P. vivax*. WM4 and WM382 are potent inhibitors of PMIX and PMX that block invasion of liver and blood stages and transmission to mosquitoes. WM4 specifically inhibits PMX whilst WM382 is a dual inhibitor of PMIX and PMX. To understand the function of PMIX and PMX proteases we identified new protein substrates in *P. falciparum* and together with detailed kinetic analyses and structural analyses identified key molecular interactions in the active site responsible for the specificity of WM4 and WM382 inhibition. The crystal structures of PMX apo enzyme and the protease/drug complexes of PMX/WM382 and PMX/WM4 for *P. falciparum* and *P. vivax* have been solved. We show PMIX and PMX have similar substrate selectivity, however, there are distinct differences for both peptide and full-length protein substrates through differences in localised 3-dimensional structures for the enzyme substrate-binding cleft and substrate interface. The differences in affinities of WM4 and WM382 binding for PMIX and PMX map to variations in surface interactions with each protease in the S' region of the active sites. Crystal structures of PMX reveal interactions and mechanistic detail on the selectivity of drug binding which will be important for further development of clinical candidates against these important molecular targets.

Introduction

Plasmepsin IX (PMIX) and X (PMX) are highly conserved aspartic proteases expressed by protozoan parasites of *Plasmodium* spp. and they play a pivotal role in processing of proteins involved in essential steps in its life cycle and consequently they are important drug targets[1, 2, 3]. Six species of *Plasmodium* spp. infect humans and *Plasmodium falciparum* is responsible for the most severe form of malaria and *P. vivax* causes the most widespread disease[4]. These parasites infect humans through the bite of an infected female *Anopheles* mosquito and the injected sporozoites rapidly migrate to the liver and infect hepatocytes in which they develop to thousands of liver merozoites. The liver merozoites are released into the blood where they invade erythrocytes, developing rapidly within them and after egress invade new erythrocytes to amplify the infection.

PMIX and PMX are responsible for proteolytic processing and activation of other proteases, as well as multiple proteins involved in development of functional liver merozoites, blood stage merozoite egress and invasion into the erythrocyte [1, 2, 3]. Consequently, inhibition of the function of PMIX and PMX with small molecule inhibitors, not only blocks the proteolytic maturation of merozoites, but also prevents their egress from erythrocytes[3]. PMX and PMIX also perform essential proteolytic functions in the sexual stages of *Plasmodium* spp. as inhibition of their protease function blocks transmission to the mosquito[1, 2, 3]. The functional importance of PMIX and X highlights the importance of these proteases as novel targets for antimalarial drug development.

In the *P. falciparum* schizont and merozoite stages PfPMX mediates a series of protease processing events, including its own activation by autocatalysis, which activates subtilisin 1 and 2 starting a proteolytic cascade required for remodelling of the parasite surface and egress from the host cell[1, 2, 3]. PfPMX also processes important ligands and proteins that are required for merozoite invasion into the erythrocyte that include Apical membrane protein 1 (AMA1), which plays an essential role in the formation of the tight junction required for merozoite invasion[1, 2, 3, 5, 6]. Additionally, the reticulocyte binding-like (PfRh) and erythrocyte binding-like (EBA) ligands are processed by PfPMX[3] and these protein families play an essential role in the initial interaction of the merozoite with the host cell and signalling within the merozoite for subsequent steps in invasion[7, 8, 9]. Other key proteolysis events mediated by PfPMX include cleavage of PfRh5 and PfRipr, two proteins that form a tripartite complex with CyRPA that binds to the receptor basigin on the host erythrocyte[3, 10].

PMIX, similarly to PMX, is autocatalytic and has been implicated in proteolytic processing of proteins in the blood stage that include Apical Sushi Protein (ASP), Rhoptry Associated Protein 1 (RAP1) and Rhoptry Neck protein 3 (RON3)[1, 2, 3]. Additionally, it processes MTRAP a protein that is required for egress of gametes during sexual differentiation and transmission of the parasite[3].

WM4 and WM382 are small molecule compounds that inhibit the function of PMIX and PMX in *P. falciparum*, *P. knowlesi* and *P. berghei* and the conservation of these proteases suggest they are potent inhibitors across *Plasmodium* spp. [3](insert Ruiz et al. ref for Med Chem). Oral administration of WM382 cures mice infected with *P. berghei* or *P. falciparum*, the latter using a humanised mouse model[3]. It also blocks transmission of both *P. falciparum* and *P. berghei* to mosquitoes and prevents blood infection from the liver stage. WM382 is a potent dual inhibitor of both PMX and PMIX and consequently, a promising lead candidate for development of new antimalarials with a novel mode of action for treatment and prevention of malaria[3].

Using recombinantly-expressed *P. falciparum* PMX, both WM382 and WM4 have been shown to be potent inhibitors of protease activity with a K_i of 0.014 and 0.45 nM respectively[3]. However, little is known with respect to the functional properties of PMIX. Additionally, there is little understanding of the molecular mechanism of binding of the dual inhibitor WM382 with PMX and PMIX or the binding of WM4 to PMX. In this work we have expressed and purified recombinant PMX and PMIX and determined 3-dimensional structures in complex with WM382 and WM4 by X-ray crystallography and homology modelling. This has allowed us to gain an understanding of the function of PMX and PMIX and unravel the molecular events involved in the inhibition of these proteases by WM382 and WM4.

Results

Identification of PfPMIX protein substrates in P. falciparum. WM4 and WM382 are inhibitors of *P. falciparum* growth because of potent inhibition of the proteolytic function of the aspartic proteases PMIX and PMX[3]. WM4 is a selective inhibitor of PMX whilst WM382 blocks both PMIX and PMX function in *P.*

falciparum. Protein substrates have been identified that are proteolytically processed by PfPMX, however, only a few have been identified that are specifically cleaved by PMIX[1, 2, 3]. To discover potential protein substrates of PfPMIX in *P. falciparum* asexual stage proteins known to be processed that have potential PMIX and X substrate recognition sequences were investigated. This identified the *P. falciparum* rhoptry neck protein 6 (PfRON6)[11], rhoptry-associated membrane antigen (PfRAMA)[12, 13] and rhoptry-associated leucine zipper-like protein (PfRALP1)[14] as potential PMIX substrates.

To test if PMIX was involved in the proteolytic processing of PfRON6, PfRAMA and PfRALP1, *P. falciparum* parasites that expressed haemagglutinin (HA) epitope-tagged forms of each protein were generated. The PMX-specific inhibitor WM4 and the PMIX/PMX dual inhibitor WM382 were used to determine if they inhibited processing of PfRON6, PfRAMA or PfRALP1 (Fig. 1). Processing of SERA5, which is mediated by SUB1, a protease activated by PMX, was used as a control (Fig. 1A)[1, 2, 3]. As expected, both WM4 and WM382 inhibit processing of SERA5 [3]. In contrast, processing of PfRON6 from p114 to p106 was inhibited by WM382 but not WM4 (Fig. 1B) suggesting PMIX and not PMX was involved. Similarly, processing of PfRAMA (Fig. 1C) and PfRALP1 (Fig. 1D) were more efficiently inhibited by WM382 compared to that observed for WM4, again indicating that PMIX was required. These results are consistent with proteolytic processing of PfRON6, PfRAMA and PfRALP1 being mediated by PMIX or that this aspartic protease activates other proteases required for these cleavage events.

Substrate specificity of PMIX and PMX. To understand the substrate specificity of these aspartic proteases in *Plasmodium* spp. active recombinant *P. falciparum* PMX (PfPMX)[3], *P. falciparum* PMIX (PfPMIX) and *P. vivax* PMX (PvPMX) were expressed and purified to enable detailed kinetic and structural analyses (Fig. S1). PfPMX expression and purification of the active mature enzyme domain has been described previously and this protease has been shown to be autocatalytic[3]. The recombinant expression products expressing the full-length zymogen form of PvPMX and PfPMIX were the active mature enzyme domains consistent with autocatalytic activity (Fig. S1)[3].

To show purified PfPMIX, PfPMX and PvPMX proteases were enzymatically active and to explore their substrate specificity, a fluorogenic assay[15] was employed to investigate their ability to cleave peptide substrates designed from known PMX and PMIX processed sites[1, 2, 3], as well as putative cleavage sites we identified for PfRON6, PfRAMA and PfRALP1 (Fig. 1E-G). PfPMX was able to cleave the peptide substrates to differing extents, as has been shown previously[3], and it was also able to cleave putative PMIX recognition peptides identified in PfRON6, PfRAMA and to some extent PfRALP1 (Fig. 1E). Similarly, PvPMX showed a near identical cleavage pattern as PfPMX in cleaving this broad range of peptide substrates indicating this recombinant protein was active and that these proteases had very similar substrate specificities (Fig. 1F).

In contrast, PfPMIX showed efficient cleavage of peptide substrates PfRh2N, PfRON3, PvRON3 and PfRAMA only and was not able to cleave those corresponding to other known PMIX or PMX processed proteins (Fig. 1G). This suggested PfPMIX either has a more restricted substrate specificity compared to

PfPMX and PvPMX, possibly due to subtle differences in the structure of its substrate binding cleft or was less efficient in its ability to cleave peptide substrates compared to full-length proteins, which may have additional localised structure to assist binding to the enzyme. PfRON3 in *P. falciparum* parasites is processed by PfPMIX[3] and the ability of this enzyme to cleave the PfRAMA and PvRAMA peptide sequence corresponding to the proposed processing site was consistent with these proteins being direct protein substrates of PMIX in the parasite (Fig. 1G). Cleavage of the PfPMX peptide substrate PfRh2N by PfPMIX suggests that this protease can process PMX protein substrates when they can be accessed by the active site. PfPMIX was not able to efficiently cleave the PfRON6 or PfRALP1 peptides or other peptides from known PMIX protein substrates such as PfASP and PfRAP1 (Fig. 1G)[1, 2, 3]. This suggests that either PfRON6 and PfRALP1 are processed by another protease that is activated by PMIX processing[1, 2, 3], or it was much less efficient at cleaving peptide substrates compared to full-length protein substrates.

To determine if PfPMIX could process full-length protein substrates, we expressed and purified *P. falciparum* Apical Sushi Protein (PfASP)[16] and PfRh5-interacting protein (PfRipr)[17] as recombinant proteins (Fig. 1H, I, J). PfASP is 83 kDa but migrates aberrantly in SDS/PAGE, likely because of the number of charged amino acids, and it has been shown to be a substrate of the protease PfPMIX in *P. falciparum* (Fig. 1I)[1, 2, 3]. PfASP is processed by PfPMIX at a known site resulting in a C-terminal p43 proteolytic fragment (43 kDa) (Fig. 1H)[3] with the fate of the N-terminal p40 fragment remaining unknown[3]. Although PfASP is a substrate for PfPMIX in *P. falciparum*[1, 2, 3], a peptide containing the cleavage motif that produces the p43 and p40 fragments was not processed by recombinant PfPMIX and inefficiently by PfPMX and PvPMX (Fig. 1E-G). Digestion of recombinant full-length PfASP using recombinant PfPMIX resulted in the production of the p43 C-terminal polypeptide fragment, as seen in the parasite[3], but unexpectedly the p40 fragment was not seen, instead a smaller fragment (p32) was observed in the SDS-PAGE band profile of the digest indicating the existence of a possible second cleavage site (Fig. 1I). Inspection of the sequence confirmed a second cleavage site that would result in a 32 kDa fragment (p32) and a much smaller 8 kDa fragment (p8). Incubation of PvPMX with full length PfASP resulted in the formation of the p43 and p40 fragments (Fig. 1J). However, the digestion involved cleavage at a single motif and did not progress further to produce the p32 fragment, as seen in the PfPMIX digestion of PfASP (Fig. 1I). This indicates the production of the p32 fragment in PfASP was the result of a two-step cleavage event mediated by PfPMIX, which occurs via the p40 intermediary fragment in PfASP. Although PvPMX can promiscuously cleave the first motif it did not cleave the second motif due to differences in substrate specificity for the substrate which can be imposed by substrate structure or a subtle difference in the structure of the enzyme binding cleft.

Following removal of its signal sequence, PfRipr is predicted to be a 123 kDa protein which is a substrate of PfPMX in *P. falciparum*[3]. PfRipr is processed by PfPMX at a single site to convert the 123 kDa protein into two polypeptides (p64 and 59 kDa) (Fig. 1H)[3]. Recombinant PfPMIX was unable to process the PfRipr cleavage motif in either a peptide (Fig. 1G) or in the full-length protein (p123) as there was no observable difference between the protein band profiles in the control lanes with the PfRipr only control

and the PfRipr/PfPMIX digest (Fig. 1J). Recombinant PfPMX and PvPMX were not effective at processing a peptide substrate with the cleavage motif for PfRipr (Fig. 1E, F). However, recombinant PvPMX was able to cleave full-length PfRipr protein (p123) into two polypeptides corresponding to p64 and p59 in *P. falciparum* parasites[3] (Fig. 1J). These results indicate that the PfRipr cleavage motif interaction with PvPMX requires additional structural interactions provided at the enzyme/protein substrate interface to enable efficient processing. These digests also validate PfRipr as a substrate of PMX but not PMIX and importantly reveal evidence that different and unique specificities can exist between these two enzymes due to protein substrate structure.

PfPMIX has subtle differences in substrate specificity for cleavage of the PfRON3 peptide. To further understand the substrate specificity of PfPMIX, PfPMX and PvPMX the ability of each protease to cleave the PfRON3 peptide sequence was tested and compared with peptides in which specific amino acids were mutated to alanine (Fig. 2A). Firstly, the cleavage site within the PfRON3 (and PfRh2N) peptides following digestion with PMIX and PvPMX were identified by mass spectrometric analysis (Fig. S2). The phenylalanine of each peptide was shown to be the P1 position with cleavage by PvPMX and PfPMIX between it and the Leucine/Isoleucine residue (P1'). This was the same cleavage position as was determined for PfPMX[3]. Both PfPMX and PvPMX gave very similar patterns of cleavage for the wild type and mutant RON3 peptides consistent with them having very similar substrate specificities (Fig. 2A). Surprisingly, the P1 phenylalanine was not essential as both PfPMX and PvPMX showed relatively efficient cleavage (RON3 m3 mutant). In contrast, the P1' and P3' isoleucine and the P4' aspartate residues were important as the ability of these proteases to process the corresponding mutant peptides was reduced (RON3 m4, m6 and m7b mutants). This data was consistent with both PfPMX and PvPMX having essentially identical substrate specificities (Fig. 1E and F).

In contrast, PfPMIX showed distinct differences with respect to its ability to cleave the RON3 mutant peptides compared to PfPMX and PvPMX suggesting subtle variance in substrate specificity (Fig. 2A). Similar to the results observed with PfPMX and PvPMX, the P1 phenylalanine residue was not essential as PfPMIX was still able to cleave the peptide, albeit weakly (m3 mutant). However, the P1' isoleucine, P2' glutamine, P3' isoleucine and P4' aspartate appear to be essential for efficient cleavage by PfPMIX (RON3 m4 - m7 mutants). This suggests that there is variation in substrate specificity for PfPMIX compared to the PMX proteases likely due to amino acid differences in the active site of the proteases (Fig. S3). Despite the contrasting ability to cleave the mutant RON3 peptides a sequence logo representation of PfPMIX cleavage sequences (Fig. 2B), compared to that for PfPMX[3], showed close similarity across the core substrate recognition sequence.

WM4 is a selective inhibitor of PMX and WM382 is a dual inhibitor of both PMIX and PMX. Previously, we have shown that WM4 is a PMX specific inhibitor whilst WM382 is a dual inhibitor of both PMIX and PMX protease function in *P. falciparum*[3]. Whilst WM4 and WM382 are potent inhibitors of *P. falciparum* growth, with an EC_{50} of 7.4 nM and 0.39 nM respectively (Fig. 2C), the molecular basis for the differential inhibition of these compounds with respect to their inhibition of PMIX and PMX function is not known. To

gain an understanding of the molecular interactions of WM4 and WM382 with PfPMX, PvPMX and PfPMIX we analysed the kinetics of inhibition (K_i) for peptide cleavage. PvPMX and PfPMIX efficiently cleaved the PfRON3 and PfRh2N peptides respectively at optima pH 5 to pH 5.5 (Fig. S4). WM4 has a similar K_i for PfPMX (0.446 nM) and PvPMX (0.408 nM) with PfPMIX having a significantly higher K_i (263 nM) with a >590-fold increase in the inhibitory effect against PfPMX and PvPMX over PfPMIX (Fig. 2C). This was consistent with WM4 specifically inhibiting PMX proteolysis but not cleavage of PMIX protein substrates in *P. falciparum*[3]. WM382 also had a similar K_i for inhibition of PfPMX (0.014 nM) and PvPMX (0.007 nM) as did WM4 consistent with them both being potent inhibitors of PMX enzyme activity. However, WM382 was also a potent inhibitor of PfPMIX (Ki = 0.4 nM), a 29-fold increase in the inhibitory effect against PfPMX over PfPMIX.

The equilibrium dissociation constant (K_D) for the affinity of WM4 binding to PvPMX (0.48 ± 0.08 nM) and PfPMX (0.39 ± 0.07 nM) was very similar as were the k_{on} (PfPMX 6.3 ±2.3 x 10^6 $M^{-1}s^{-1}$, PvPMX 7.6 ± 5.4 x 10^6 $M^{-1}s^{-1}$) and k_{off} (PfPMX 2.4 ± 0.8 x 10^{-3} s^{-1}, PvPMX 3.4 ± 2 x 10^{-3} s^{-1}) rates (Fig. 2D and F, Table S1). This was consistent with the conservation of the active site of these proteases (Fig. S2) and showed that this compound bound strongly to these enzymes. In contrast, the K_D of WM4 for PfPMIX (77 ± 13 nM) showed a 160-fold lower affinity of binding with the k_{on} (6.0 ± 3.1 x 10^5 M^{-1} s^{-1}) and k_{off} (4.7 ± 3.0 x 10^{-2} s^{-1}) rates also significantly lower (Fig. 2H, Table S1). These results are consistent with WM4 being a specific inhibitor of PfPMX but not PMIX protease function in *P. falciparum* parasites[3]. WM382 bound the three enzymes with very high affinity, with a K_D of <0.1 nM. The dissociation curves were flat for all proteases and it was not possible to determine k_{off} rates and therefore a K_D as the response did not decrease below 5% during the 25 min dissociation phase (Fig. 2E, G and I). This data was consistent with the potent enzyme inhibition observed and showed there were no measurable differences in the K_D for WM382 between PfPMX, PvPMX or PfPMIX. These results also suggest that the high potency of WM382 for inhibition of PfPMX, PvPMX and PfPMIX was driven to a great extent by the very slow off rates for binding of the compound.

Structure of P. falciparum **PMX.** To understand the structural basis for the specificity for WM4 inhibition of PMX compared to the dual specificity of WM382 to inhibit both PMIX and PMX crystal screens were performed with the apo enzymes as well as in complex with WM4 and WM382 for PfPMX, PvPMX and PfPMIX. Diffracting crystals were obtained for the PfPMX apo protease as well as the protein/drug complexes PfPMX/WM382, PvPMX/WM382 and PvPMX/WM4.

A crystal structure of the apo protease PfPMX was obtained at a resolution of 1.85 Å (Fig. 3A and B). PfPMX has a canonical aspartyl protease fold with a crescent shape and a predominantly b-sheet core (Fig. 3B)[18, 19]. The N- and C- terminal subdomains are anchored via a six stranded interdomain b-sheet. The uppermost b-strand (PfPMX F237-P240) of this sheet arises from the cleavage and removal of the prodomain and the subsequent relocation of the N-terminus to enable association with the enzyme domain[20]. Subsequently, a mobile loop is formed in the processed N-terminal (PfPMX F237-L252) region

and anchored to the mature enzyme structure by incorporation into the b-sheet (Fig. 3B). This loop forms the edge of a sub-pocket within the S3 substrate binding site and its importance in inhibitor binding is discussed below. A single hairpin loop is centrally located on the outside of the substrate binding cleft (Fig. 3. A and B). The loop between residue Asn345-Asp352 had poor electron density and could not be structurally determined in PfPMX. These missing residues are located at the edge of the active site cleft and thus presumably not involved in ligand binding.

Aligning the apo PfPMX enzyme structure with that of another member of the plasmepsin family, plasmepsin V (PMV) in complex with a peptidomimetic inhibitor WEHI-842 (not shown in schematic for simplicity), shows that the PfPMX loop (residues Asn345-Asp352) has a closed conformation without requiring the engagement of a substrate or inhibitor (Fig. 3C)[19]. PfPMX consists of the core aspartic protease structure and lacks other domains present in PvPMV such as the two b-barrels present at the bottom of the structure and the 'nepenthesin 1-type' aspartyl protease (NAP1) fold (Fig. 3C). These sequences in PvPMV are likely involved in protein-protein interactions and access to the protease active site and the lack of these shows that PfPMX does not require additional domains to perform the basic function of proteolysis for its target protein substrates.

A modeled structure for PfPMIX was generated using the PfPMX structure and comparison has revealed that the key structural and functional residues in the active site are located in similar positions in the PfPMIX model (Fig. 3. D). PfPMIX has a 59 residue insert (I431-N490) that is not shown and as this feature and structure is unique to this protease it could not be accurately modeled (Fig. 3D, S2). This insert occurs within four residues on the N-terminal side of the active site amino acid residue D457 and its influence on substrate binding has not been determined to date. Although the modeled structure for PfPMIX shows similarity to that found for PfPMX, its electrostatic surface was predicted to have a charge reversal around the location of its S3 pocket, which could generate subtle changes in the substrate specificities between each of these enzymes (Fig. S5).

PMX/inhibitor structure and interactions that mediate inhibitor binding affinity and specificity. Structures were obtained for PfPMX in complex with WM382 (resolution 2.76 Å) as well as PvPMX in complex with WM382 (resolution 2.22 Å) and WM4 (resolution 3.35 Å) (Fig. 4 and Table S2). The structure of PvPMX had similarity to that obtained for PfPMX including the basic architecture of the active sites and binding of WM382, although there are specific regions in the catalytic cleft that show localised structural movements due to drug binding (discussed below) (Fig. 4). Both WM382 and WM4 inhibitors align with the active site residues and are positioned between the inner and outer (S2 flap) surfaces of the substrate binding pocket (Fig. 4A, D and G). The structures for the protease-inhibitor complexes for PfPMX/WM382, PvPMX/WM382 and PvPMX/WM4 showed that the models for the inhibitors matched the observed electron density found within the substrate binding pocket as shown in the OMIT diagrams (2Fo-Fc density contoured at 1.0 σ) (Fig. 4B, E and H).

WM4 and WM382 share a common template but they have different moieties projecting from them designed to promote enhanced interactions within the substrate binding pocket. These subtle structural

variations have led to the observed differences in binding affinity and substrate specificity for each of these compounds with PfPMX and PvPMX (Fig. 4C, F, I) and subsequently PfPMIX. Hydrogen bonds are the strongest surface interactions occurring between the active site of the corresponding protease and the inhibitors within the structures of these complexes. Within the PvPMX-WM4 complex (Fig. 4I), hydrogen bonding occurs in the S1 pocket between the hydrogen atoms of an amine and imine group from the 'warhead' on WM4 and the active site aspartic acid residues in PvPMX (D231 and D421) (Fig. 4I). An additional hydrogen bond also occurs between the main chain carbonyl group of G423 and the amide hydrogen of the carbonyl amide moiety on WM4. Hence, hydrogen bonds tether WM4 to the wall of the S1 pocket at the back of the substrate binding cleft.

The hydrogen bonding pattern observed between WM382 with PfPMX and PvPMX was identical in both structures (Fig. 4C and F). The pattern contains the same hydrogen bonds observed for the PvPMX/WM4 structure (Fig. 4I) but has an additional bond occurring between the carbonyl of the carbonyl amide moiety of WM382 and the hydroxy hydrogen of a serine located in the S2 flap at the front of the substrate binding cleft (PfPMX S313 and PvPMX S278). This additional hydrogen bond enables tethering of WM382 to the front S2 pocket in addition to the back surface of the S1 pocket in the substrate binding cleft in PfPMX and PvPMX (Fig. 4C and F). This same hydrogen bond does not seem to form with WM4 as the positioning of the phenyl moiety in the S'1 and S'2 pockets is such that it results in a more downward placement of the central aromatic ring, shared in both compound structures, than observed in WM382. This slight change in relative placement (1.7 Å) has a flow on effect, with the carbonyl of the adjacent carbonyl amide moiety now being too far away from S278 to enable the formation of a hydrogen bond similar to one observed in WM382. Interestingly, the modeled structure for PfPMIX in complex with WM382 has a Ser to Thr amino acid substitution in the same position in the flap of the S2 pocket suggesting this additional hydrogen bond can occur in the PfPMIX/WM382 complex (Fig. S6).

Amino acid residues positioned within 4 Å of WM4 and WM382 in the PvPMX/inhibitor structures were visualized by mapping onto a surface representation of the structures tabled with their location in the substrate binding cleft and color-coded as common to both inhibitors and unique to a specific inhibitor (Fig. 5). The common interactions (orange) occur about the active site aspartic acid residues and the compound warhead in the S1 and S2 pockets (Fig. 5). The parent WM4 inhibitor (cyan) has specific interactions (green) which occur predominantly in the S1'/S2' pockets via a unique phenyl group protruding into this area (Fig. 5B and D). The binding affinity (K_D), as determined by SPR, for binding of WM4 to the PvPMX active site was 0.48 nM (Fig. 2D). Interestingly, the WM382-specific interactions (magenta) are located towards the opposite end of the substrate binding cleft, in the S2, S3 and S3 sub pocket areas (Fig. 5A and C). This inhibitor has a methylated chromane moiety that enables greater extension and interaction with residues in this region compared to the a-methyl benzyl moiety located in the same position in WM4. Furthermore, WM382 was positioned such that an additional hydrogen bond occurred between Ser278 (S2 pocket) and the carbonyl of the carbonyl amide moiety, which engages the flap and tethers WM382 between the front and back surfaces of the catalytic cleft and explains the

stronger binding affinity of WM382 compared to WM4. This was reflected in the K_D values determined by SPR for binding of WM382 to PvPMX and PfPMX (K_D <0.1 nM).

Although WM4 and WM382 are both capable of inhibiting PfPMX function in *P. falciparum* only WM382 shows a dual specificity that includes potent inhibition of PfPMIX[3]. Based on the results above, these differences in specificity are due to differences in the structures for the substrate binding cleft for PfPMIX and PfPMX or PvPMX. Given that the K_D for WM4 interacting with PfPMIX was 77 nM, 160-fold weaker than that for PfPMX (0.39 nM) and PvPMX (0.48 nM), this indicated that WM4 has decreased interaction with the surface in the S1'/S2' pockets of PMIX and is the basis of the unique PMX specificity of this inhibitor compound. Interestingly, a large 59 amino acid loop, with unknown structure, is inserted between the two sub domains of the mature PfPMIX enzyme (Fig. S3). This loop attaches, at the C-terminal end, within six residues of the active site D495 and may destabilize or be responsible for a change in surface topography in the S1'/S2'area.

The binding affinity of WM382 for PfPMIX was the same as that obtained for PvPMX and PfPMX (ie. K_D <0.1 nM). In the PMX structures, WM382 interacts with the S1-S3 pockets and was tethered via four hydrogen bonds to the front and back of the substrate binding cleft. In a modeled structure for PfPMIX (based on the structure of PvPMX/WM382) the same hydrogen bonding pattern can be predicted with a T293 replacement for the PvPMX S278/PfPMX S313 in the flap at the front of the substrate binding pocket. The model predicts a similar distribution of weaker dispersion forces about the S1 to S3 pockets. Collectively this supports a similarity in this region of the substrate binding surface in PMX and PMIX and the basis for the dual specificity observed for WM382 inhibition of these two proteases.

The localized structural response of plasmepsin X to enable inhibitor binding. For the PfPMX and PvPMX structure the S2 flap and the loop of the S3SP showed significant changes in conformation for inhibitor binding (Fig. 6). In the PfPMX apo structure the S2 flap, particularly between residues F311 to G314, was found to be twisted almost perpendicular to the substrate binding cleft resulting in F311 being orientated into and S313 (not shown) orientated away from the empty cleft. Meanwhile the S3SP loop (H242 to F248) has a width from the Q247Ca to the L243Ca of 6.6 Å and residues within this loop have an outward projection (Fig. 6A). Entry of the inhibitor WM382 into the substrate binding cleft of PMX appears to have occurred from the S' side of the cleft because of the unilateral change in orientation in the most affected residues. As a result, the amino acid F311 has moved 4.2 Å from where it was positioned in the apo structure and instead of projecting inward toward the cavity space of the cleft, the side chain has been reorientated toward the S2 flap to provide sufficient spatial separation from inhibitor WM382. Amino acid residue S313 was also repositioned via approximately a 90˚ rotation and a 4.8 Å directional shift in the hydroxy group of this residue. This structural change subsequently enables a hydrogen bond to occur between inhibitor WM382 and the hydroxy moiety of S313 as discussed previously (Fig. 4C).

The positioning of the WM382 warhead for interaction with the active site aspartic acid residues of PfPMX also requires the S3SP loop to be displaced further out of the cleft as shown by the 3 Å shift to

the right and the width of the loop (Q247Ca to L243Ca) was compressed by 1.2 Å (Fig. 6A). Otherwise, the methylated chroman moiety of WM382 would collide with residues forming the S3SP loop. Furthermore, the outward projecting residues of the S3SP loop observed in the PfPMX apo structure are found to be orientated more upward and toward the inside of the loop in the PfPMX/WM382 structure. This reorientation of the S3SP residues enables the loop to be stabilized by an increased number of hydrogen bonds (Fig. 6 and Table S3).

As discussed previously, the S3SP loop is believed to be obtained from the rearrangement of the unstructured residual pro-sequence remaining after the autolytic cleavage events required to activate PMX, via a similar process described for other aspartyl proteases (autolytic activation)[20]. In the PfPMX apo structure the S3SP loop was quite mobile and has limited rigidity due to the low number of observed hydrogen bonds between residues within the loop (Fig. 6D and Table S3). In comparison, the structure obtained for PfPMX/WM382 complex has eight hydrogen bonds within the loop structure. This has arisen due to inhibitor induced compression of the loop and the inward reorientation of loop residues (Fig. 6E). The hydrogen bond pattern is three dimensional and not only increases the rigidity within the loop but also tethers the loop to a region outside via a hydrogen bond between Q247 and D245 (Fig. 6E and Table S3).

The S3SP loop structure for the PvPMX/WM382 complex has the same number of hydrogen bonds as the S3SP loop in PfPMX/WM382 complex but the hydrogen pattern was slightly different due to the influence of D323 (PvPMX) rather than S359 (PfPMX) as the external tethering point for the S3SP loop (Fig. 6F and Table S3). The loop structure in the PvPMX/WM4 complex has six hydrogen bonds and incorporates both internal and external hydrogen bond tethering points for increased loop rigidity. The a-methyl benzyl moiety of WM4 does not protrude as far into the S3SP as the methylated chromane moiety of WM382 and likely influences positioning of the D210 residue in the structure of the PvPMX/WM4, as two hydrogen bonds involving Q212 and D210 are not observed. Hence, the S3SP loop becomes stabilized by inhibitor displacement and loop compression with reorientation of loop residues that favor hydrogen bond formation leading to increased loop stability. This region was not obvious in the structure of the apo form of PfPMX. The S3SP is consequently, an important region for increasing affinity of binding for members of this inhibitor family to PMIX and PMX via hydrogen bond formation and increased Van der Waals interactions.

Discussion

Plasmepsin IX and X in *Plasmodium* spp. are essential aspartic proteases that proteolytically process many different proteins required for parasite egress, invasion and development of liver, blood and transmission stage parasites and consequently are important drug targets for development of novel antimalarials[1, 2, 3]. WM4 and WM382 are lead compounds for development of antimalarials with a mode of action that can target either PMIX and X together or more specifically PMX alone [3]. The mechanism by which these compounds can differentially inhibit the function of these two aspartic proteases has been unknown. In this study we have obtained the crystal structures of PMX as an apo enzyme and in complex

with WM4 and WM382 as well as performed detailed enzyme kinetic and binding analyses to identify the different molecular interactions of these compounds in the active site that explain the specificity of drug inhibition for the different proteases.

The proteins PfRON6, PfRAMA and PfRALP1 have been identified as substrates of PfPMIX in *P. falciparum* parasites increasing those known to be processed by this protease. The ability of WM382 (PMIX and PMX dual inhibitor) to specifically inhibit processing of these proteins suggested they are direct protein substrates of PfPMIX. However, it was possible this aspartic protease activated another intermediate protease that was directly responsible for processing of final substrates, as is the case with respect to the activation of SUB1[1, 2] and SUB2[3]. The identification of PMIX amino acid recognition sites in those proteins that once cleaved correspond to the observed molecular weight of the proteolytic processed polypeptides for each protein in the parasite, and the ability of these peptides to be cleaved by either PfPMIX, PfPMX or PvPMX supports them as true PfPMIX protein substrates. Conditional knockout of the gene encoding PMIX in *P. falciparum* blood stages has shown that the function of this protease was essential[1, 2] indicating that proteolytic processing of at least some of these protein substrates is required for their function. In *P. falciparum* the PfPMIX processed protein PfRAMA is essential for correct trafficking of a subset of rhoptry proteins and a conditional gene knockout results in dysmorphic rhoptries lacking a neck region and merozoites that are unable to invade erythrocytes[12].

Our results show that PMIX and PMX have similar peptide substrate selectivity, however, there are clear differences in their ability to efficiently process different full-length protein and peptide substrates. Recombinant PfPMIX can process full-length PfASP but not the peptide corresponding to the cleavage site suggesting that additional interactive structural elements are required for recognition and effective cleavage of these motifs, which are provided by the protein. PMIX was also not able to proteolytically process recombinant PfRipr, a known PfPMX substrate[3]. Interestingly PvPMX, in addition to cleaving full-length PfRipr, could process the recombinant full-length PfASP but it did so less efficiently and incompletely compared to PfPMIX, with only one of the two cleavage motifs processed. It is likely the properties of the protein substrates and the surface structure around and in the active site of both PMIX and PMX are responsible for these subtle differences. These observations indicate that the distinct subcellular localisation of PMX in the micronemes and PMIX in the rhoptries[1, 2] is an important aspect for the apparent protein substrate selectivity of these aspartic proteases. This raises the question as to why *Plasmodium* spp. require two aspartic proteases expressed in merozoites with similar substrate selectivity? The most likely answer is that since PMX and PMIX substrates are localised to both the micronemes and rhoptries, two aspartic proteases are required to be independently trafficked to these organelles to process those substrates.

WM4 and WM382 are a promising novel class of compounds being developed as antimalarials and the fact that WM382 has dual activity against both PMIX and PMX is an invaluable property, as it results in a high bar for the development of resistance by *P. falciparum*[3]. Additionally, the development of WM4 that is specific for PMX has provided a useful chemical tool to interrogate the role of both PMIX and PMX in

parasite biology. Analysis of the structures obtained for PMX apo and PMX/inhibitor complexes have shown how a PMX specific (WM4) and a dual PMIX and PMX (WM382) inhibitor are positioned within the enzyme substrate binding pockets and the changes required in this localised environment to accommodate inhibitor binding. WM4 specific inhibition of PMX is due to unique interactions occurring in the S1’ and S2’ substrate binding pockets. The decreased ability of WM4 to block PMIX activity indicates this protease is structurally different in the S’ region of its substrate binding pocket. Comparatively, the structures for the PfPMX/WM382 and PvPMX/WM382 complexes reveal that this inhibitor does not extend significantly into the S’ region, as per WM4, but has more surface interactions in the S2’ and S3’ pockets in addition to those that are common to both inhibitors.

The design of WM382 enables the formation of an additional hydrogen bond, which occurs between a serine in the S2 flap, at the front of the catalytic cleft, and carbonyl of a carbonyl amide group in WM382. This engagement of the S2 flap results in tethering of WM382 between the inner and outer surfaces of the substrate binding cleft. As a result, a much stronger interaction occurs between PMX and WM382 which is reflected in the PMX/WM382 binding affinity in comparison to that obtained for PMX/WM4. A similar binding affinity was observed for the PMIX and WM382 interaction and implies this inhibitor is binding to a region of the substrate binding surface of PMIX similar in structure to the corresponding region in PMX.

Analysis of the structures obtained for PMX apo and PMX/inhibitor complexes have shown how a PMX specific (WM4) and a dual PMIX and PMX (WM382) inhibitor are positioned within the enzyme substrate binding pockets and the changes required in this localised environment to accommodate inhibitor binding. In the first instance, the PMX specific inhibition by WM4 occurred because of unique interactions occurring in the S’1 and S’2 substrate binding pockets. The decreased ability of WM4 to block PMIX activity indicates this protease is structurally different in the S’ region of its substrate binding pocket. Comparatively, the structures for the PfPMX/WM382 and PvPMX/WM382 complexes reveal that this inhibitor does not extend significantly into the S’ region, as per WM4, but has more surface interactions in the S2 and S3 pockets in addition to those that are common to both inhibitors. Additionally, PMX makes similar localised changes to its conformation and stability to accommodate both WM4 and WM382. The S2 flap was pushed aside and a mobile loop, which has been reorientated after autolytic activation of PMX, becomes compressed and displaced. This enables increased hydrogen bonding within and external to the loop resulting in increased stability and formation of a new surface not present in the apo structure of PMX. This surface could be targeted/engaged by informed moiety design on the core structure of this family of inhibitors and used to increase the affinity of new generation of dual inhibitors binding to this region of the substrate binding pocket.

Methods

Ethics Statement. Use of human blood and serum was approved by the Walter and Eliza Hall Institute of Medical Research Human Ethics committee under approval number 19-05VIC-13. Use of animals was

approved by the Walter and Eliza Hall Institute of Medical Research Animal Ethics Committee under approval numbers 2017.014 and 2019.013.

Parasite culture. *P. falciparum* asexual blood stage parasite cultures and the parasite lines derived from these by genetic manipulation were grown in *in vitro* culture [21] in O^+ erythrocyte (Australian red-cross bloodbank, South Melbourne, Australia) at 4% hematocrit in Roswell Park Memorial Institute (RPMI) 1640 medium supplemented with 26 mM 4-(2-hydroxyethyl)piperazine-1-ethanesulfonic acid (HEPES), 50 µg/ml hypoxanthine, 20 µg/ml gentamicin, 0.2% NaHCO3, 0.25% Albumax IITM (Gibco), and 5% heat-inactivated human serum. Cultures were incubated at 37^{o}C in a mix of 94% N_2, 1% O_2 and 5% CO_2.

Parasite lines expressing HA-tagged proteins. Transgenic parasite lines were made using the CRISPR-cas9 system as previously described [3]. Guide oligos designed to induce a double-stranded break in the corresponding genomic positions were InFusion cloned into pUF1-Cas9G: RON6: CCATCATCTCTATTGTCCTA; RAMA: GATGAAGAATTACCAAGTGA; and RALP1: TAAAGCAGCGAATGGTAAGA (for C-terminal tagging). The strategy involves the generation of a guide plasmid and a plasmid that replaces the endogenous target gene with a tagged version (the homology-directed repair or HDR plasmid). The HDR plasmid was made in 3 steps (for RON6 and RAMA) or 2 steps (for RALP1), with 5’ and 3’ flanks (~500 bp upstream or downstream from the guide sequence) amplified from 3D7 genomic DNA (or synthesised by Genscript) and a codon-optimised target gene sequence (Genscript) downstream of the Cas9 cleavage site fused to the 5’ flank. This was assembled in a modified p1.2 plasmid encoding WR99210 resistance. 50 µg of linearized HDR plasmid and 100 µg of circular guide plasmid were transfected simultaneously into E64-treated schizonts. Parasites with an integrated drug-resistance cassette were selected and maintained on 2.5 nM WR99210.

Sequence	Name	Description
CCATCATCTCTATTGTCCTAtgg		RON6 guide + PAM
gcggccgcgttaaaagacatatcggaaaatgct	TT1290	RON6 5' flank, forward
tacgtattcccataatattggaaacatataca	TT1291	RON6 5' flank, reverse
gaattcacagggaaaacacaatgataaataatat	TT1292	RON6 3' flank, forward
ggtacctgaatatttttttatttctctcaggt	TT1293	RON6 3' flank, reverse
GATGAAGAATTACCAAGTGAagg		RAMA guide + PAM
gcggccgccatataatacattcaatggtacta	TT1159	RAMA 5' flank, forward
tgtacatctagaaggtcttctttattttc	TT1160	RAMA 5' flank, reverse
gaattcacaaaaagtaaaaggaaaatcattcg	TT1161	RAMA 3' flank, forward
ggtaccgttcatttgtttctttcatatcttcgct	TT1162	RAMA 3' flank, reverse
TAAAGCAGCGAATGGTAAGAagg		RALP1 guide + PAM
gaattcaaaaatggggtttttgtaaaattga	TT1163	RALP1 3' flank, forward
ggtacccgttgagaactttcattatcacca	TT1164	RALP1 3' flank, reverse

Protease processing inhibition assays in P. falciparum **parasites.** Processing inhibition assays were performed essentially as previously described [3]. Protease inhibitors were added to synchronised late trophozoite/early schizont cultures, then passed over LD or LS magnetic columns (Miltenyi Biotech) to remove uninfected erythrocytes. WM4 and WM382 were added at 40 nM and 2.5 nM final concentrations respectively. A control dish without protease inhibitors was included. Parasites were eluted from columns with complete RPMI 1640 culture medium with inhibitor at the same concentration. Eluted parasites were adjusted to $5x10^6$ schizonts/ml and 150 ml added per well of a 96-well flat-bottomed culture dish. The parasites were cultured for 16 hr and a representative well smeared for Giemsa staining, to ensure that rupture had occurred normally (control well) or that rupture had been blocked (WM4, WM382 conditions). Parasites were centrifuged at 10000g / 10 min to collect merozoite and supernatant fractions. Proteins from both fractions were added to Reducing sample buffer and separated on 4-12% or 3-8% acrylamide gels (NuPAGE, Invitrogen) for subsequent immunoblots.

Expression, purification and crystallisation of apo PfPMX, PvPMX and PfPMIX. The apo form of PfPMX was expressed as previously described[3]. In short, PfPMX was expressed for 72 hr at 28°C in *Spodoptera frugiperda* (Sf21) cells transfected with Baculovirus. The PfPMX protein was harvested by centrifugation at 4°C, 12,000 x g for 15 min and purified by nickel affinity chromatography using a flow gravity column and eluted in 15 mM imidazole increments. PfPMX was subsequently dialysed against 4 L 20 mM Tris pH 7.5, 150 mM NaCl, and concentrated using a 30 kDa concentrator. The PfPMX autocatalysis was promoted by diluting PfPMX into 50 mM sodium acetate pH 4.0, 150 mM NaCl for 20 min. at 37°C. The

autocatalysis was concluded by the addition of 1 M Tris pH 8 until pH 7.5-8 was reached. Lastly, the processed PfPMX was further purified by size exclusion in 20 mM Tris pH 7.5, 150 mM NaCl using a HiLoad® Superdex 16/600 200 pg (Cytiva) column on an Akta Pure chromatography system.

To express recombinant PfPMIX the gene sequence (212KCD…NNL647) was recodoned for insect cell expression and synthesised by GenScript and subcloned into the p1TF vector that enabled expression in insect cells. For expression in mammalian cells the PfPMIX gene was was synthesised by GenScript and subcloned into a pCDNA 3.4 expression vector containing a N-terminal IL-2 signal sequence followed by a consensus Kozak sequence. PfPMIX was expressed in CHO cells as described [22]. In summary, sterile 1 mg PfPMIX DNA per mL expression culture was transiently transfected into CHO cells using the ExpiCHO Expression System (Thermo Fischer Scientific) and expressed at 37°C and rotated at 120 RPM for 8 days. The suspension culture was harvested by centrifugation at 4000 x *g* for 30 min at 4°C and then dialysed against 20 mM Tris pH 7.5, 300 mM NaCl overnight at 4°C. PfPMIX was subsequently purified by gravity flow nickel affinity chromatography and eluted by 15 mM imidazole increments. This was followed by ion exchange chromatography on a HiTrap® SP HP column (Cytiva) using 20 mM Tris pH 7.5, 300 mM NaCl and 20 mM Tris pH 7.5, 1.2 M NaCl as binding and elution buffers, respectively. The PfPMIX was flash frozen and stored at -80°C until further use.

PvPMX (residues H27–E545) was recodoned for insect cell expression (Bioneer), then cloned into an insect cell expression vector bearing an N-terminal gp67 signal peptide and a C-terminal fusion tag comprising a tobacco etch virus (TEV) protease-cleavage site and a FLAG tag. This was expressed in Sf21 insect cells. An N-terminally processed form of the expected recombinant zymogen was purified initially from cell supernatant using anti-FLAG M2-agarose (Sigma). Pooled fractions were concentrated, and further purified using Gel-filtration chromatography (Superdex 75, GE Life Sciences) in 20 mM Tris, pH 7.2, 100 mM NaCl, which resulted in pure and stable protein that was concentrated for crystallization and other biochemical and biophysical characterisations.

Crystallisation trials and protein structure analysis. Purified PfPMX was used for crystallisation trials alone and in complex with WM382. Apo crystals grew in 0.01 M zinc chloride, 0.1 M sodium acetate pH 5.0, 20% w/v PEG6000. These crystals were used as a seed stock and the crystal conditions repeated. Larger crystals grew in 25% w/v PEG1500, 10% w/v SPG pH 4.0 within 5 days. For PfPMX in complex with WM382 crystals grew in 12.5% v/v 2-methyl-2,4-pentanediol, 0.1M bicine-tris pH 8.5, 2.85% v/v diethylene glycol, 6.35% v/v pentaethylene glycol, 12.5% w/v polyethylene glycol 1000, 12.5% w/v polyethylene glycol 3350, 5.2% v/v tetraethylene glycol, 4.1% v/v triethylene glycol.

Extensive soaking and co-crystallisation trials of apo PfPMX with WM382 failed to produce protein crystals. Diffracting crystals of PfPMX complexed with WM382 were obtained from PfPMX expressed in the presence of WM382 in insect cells, from which 70 kDa protein band was detected by SDS-PAGE. This corresponds to the inactive unprocessed PfPMX. Purification by ion exchange chromatography resulted in highly pure uncleaved PfPMX/WM382 complex. Size exclusion chromatography of this material resulted in a mixture of unprocessed and processed PfPMX preparation. Interestingly, only this mixed

PfPMX preparation resulted in protein crystals after 30 days and these diffracted to 2.76 Å. The structure of PfPMX complexed with WM382 structure was the same sequence length as the apo PfPMX. Our unpublished data suggest that PfPMX gets cleaved at neutral pH after a lengthy incubation time. Thus, it is possible as PfPMX+L-312 got cleaved, the optimal protein concentration for crystal nucleation was eventually reached.

The crystals were shot with the MX2 beamline at the Australian Synchrotron (Melbourne, Australia). The protein structures were determined by molecular replacement with the Autorickshaw server [23] using rat cathepsin (5ux4.pdb) as the search model. Subsequently the determined structures were refined using the Coot [24] and Phenix [25] software packages. The OMIT diagram was generated using Phenix composite OMIT Map.

PvPMX was co-crystallized with various inhibitors in 2 M ammonium sulfate, 0.1 M sodium HEPES pH.5, 2% (v/v) PEG400 and 1 mM Anderson-Evans polyoxotungstate. Crystals were frozen in well solution supplemented with 20% glycerol. Data were collected at the Australian Synchrotron beamline MX2 at 100 K and processed with XDS [26, 27], Pointless[27] and Aimless [28]. Subsequent structures were solved by molecular replacement using the Auto-Rickshaw server[23], which used PfPMX-apo as a search model, with residues surrounding the catalytic site mutated to Ala. Further rounds of building and refinement with Coot[24] and Phenix[29] yielded the final model.

Accession codes. Coordinates and structure factors for *P. vivax* and *P. falciparum* PMX have been deposited in the Protein Data Bank under accession codes (will be added). During manuscript preparation we noted a yet to be published released X-ray structure for PfPMX PDB accession code 6ORS whose backbone conformation resembles the structures we determined (RSMD=0.862 (243 to 243), 315 residues, α chain carbons (PfPMX 233E-570K) (https://www.rcsb.org/structure/6ORS) deposited by Seattle Structural Genomics Center for Infectious Disease).

PMIX modelling. MOE molecular modelling package (MOE2019.01, Chemical Computing Group, Montreal, Canada) was used for homology model building. The PfPMIX and PvPMIX models were built using the crystal structures of PfPMX and PvPMX, respectively, as templates. The sequence identities are 45% for PfPMIX vs PfPMX, and 47% for PvPMIX vs PvPMX.

Expression of recombinant PfASP and PfRipr protein. The gene encoding PfRipr (residues 20 to 1086) was sub-cloned into pAcGP67a with a C-terminal His-tag. The construct was expressed in Sf21 cells and secreted into the medium as soluble protein. Medium was dialysed into 20 mM Tris pH 8, 150 mM NaCl. Imidazole was added to 10mM final concentration and PfRipr was purified by NiNTA Superflow resin (Qiagen) and eluted in 20 mM Tris pH 8, 150 mM NaCl, 500 mM Imidazole. The sample was further purified via size eclusion chromatography, using a HiLoad Superdex 200 16/600 column (Cytiva). Fractions containing PfRipr were pooled and concentrated to 1 mg/mL for protease assays.

The gene for *P. falciparum* (3D7) Apical sushi protein (corresponding to residues E22 to S710) was expressed as protein with a C-terminal fusion tag comprised of a TEV cleavage motif and flag peptide. Apical sushi protein (ASP) was expressed in HEK exp293F and the crude supernatant purified initially using M2 anti-flag affinity resin. Fractions containing the desired expression product, as determined by SDS_PAGE analysis, were pooled and dialysed against 20 mM Bis-Tris pH 6.5/20 mM NaCl. The protein pool was then further purified using Strong Anion Exchange chromatography (SAX). ASP was eluted from a Hitrap column using a gradient from 0 to 50%B. Where Buffer A was 20 mM Bis-Tris pH 6.5 and Buffer B=A+1 M NaCl. Selected fractions were analyzed using SDS-PAGE and the relevant fractions pooled. SEC purification of the SAX pool was conducted using a Superdex200 column and buffer comprised of 20 mM Bis-Tris pH6.5/150 mM NaCl. Fractions were analyzed by SDS-PAGE and fractions pooled to give a solution containing highly purified PfASP.

Digestion of ASP and PfRipr proteins with PvPMX and PfPMIX. Individual digests were of 20 ml total volume and comprised of an enzyme:substrate w/w ratio of 1:40 in a buffer comprised of 20 mM Bis-Tris pH 6.50/150 mM NaCl. Digests or controls (individual components of the digest mixtures) were incubated overnight at 37^0C. Samples were then centrifuged and run on reducing SDS-PAGE for analysis.

FRET based assay for PfPMX, PvPMX and PfPMIX cleavage of peptide substrates. Synthetic FRET based peptide substrates corresponding to *P. falciparum* and *P. vivax* cleavage sequences from PMX and PMIX protein substrates were synthesized by ChinaPeptides (listed below). Substrate cleavage efficiency assays were performed by incubating fluorogenic peptides (20 µM) with and without 10 nM PfPMX, PvPMX or PMIX in 20 µl assay volume in black low volume 384 well assay plate (Corning #4514). Enzymes and peptide substrates were prepared in 25 mM sodium acetate (pH 5.5) and 0.005% Tween-20 for PfPMX and PvPMX assays and in the same buffer supplemented with 100 mM sodium chloride for PfPMIX assay. Reactions were allowed to proceed at 37^oC for 4 hr. Samples were excited at 340 nm and fluorescence emission measured at 480 nm using a PHERAstarFSX plate reader (BMG Labtech).

FRET based Peptide substrates	Source	Protein identifier
DABCYL-HSFIQEGKEE-EDANS	China Peptides	PfRh2N
DABCYL-GTASLVQITQYE-EDANS	China Peptides	PfRh2C
DABCYL-KPFFFIQLNTE-EDANS	China Peptides	PfRh1
DABCYL-KNVNFLQYHFE-EDANS	China Peptides	PfRh5
DABCYL-GNISMLEIQNEE-EDANS	China Peptides	PfRipr
DABCYL-GFSSESFLENKG-EDANS	China Peptides	PfRAP1
DABCYL-GFSSESFAANKG-EDANS	China Peptides	PfRAP1 mutant
DABCYL-GSMLEVENDAEGE-EDANS	China Peptides	PfSUB1
DABCYL-GSMAAVENDAEGE-EDANS	China Peptides	PfSUB1 mutant
DABCYL-RILSFLDSRIE-EDANS	China Peptides	PfEBA175
DABCYL-NRNSFVQRSYE-EDANS	China Peptides	PfEBA181
DABCYL-NRNAFVARSYE-EDANS	China Peptides	PfEBA181 mutant
DABCYL-HAFIAEGKEE-EDANS	China Peptides	PfRh2N mutant
DABCYL-EKFLSLLQLNLKE-EDANS	China Peptides	PfASP
DABCYL-ILNSFVQINSE-EDANS	China Peptides	PfRh4
DABCYL-ILNAFVAINSE-EDANS	China Peptides	PfRh4mut
DABCYL-KEISFLERRE-EDANS	China Peptides	PfRON3
DABCYL-KEIAFLARRE-EDANS	China Peptides	PfRON3mut
DABCYL-KFNSLSENEDNE-EDANS	China Peptides	PfEBA140
DABCYL-GKLRSTMLEVE-EDANS	China Peptides	PvSUB1
DABCYL-GESFIDVKNAE-EDANS	China Peptides	PvPMX
DABCYL-SQSSFVQRSKE-EDANS	China Peptides	PfROM1
DABCYL-KFLSLLELKSE-EDANS	China Peptides	PvASP
DABCYL-GATSFIQSRE-EDANS	China Peptides	PfGAMA
DABCYL-NGVSFLQKKE-EDANS	China Peptides	PvRON3
DABCYL-THTSFLQNCTE-EDANS	China Peptides	PfRON6
DABCYL-YEESFLQNDE-EDANS	China Peptides	PfRAMA
DABCYL-VTHSFLDMSKE-EDANS	China Peptides	PfRALP1

K_m determination for plasmepsin proteases. The K_m determination for PfRh2N and PfRON3 substrates was conducted in 20 µl total volume with 0.3 nM PfPMX, PvPMX or PfPMIX and peptide substrate concentration series starting at 40 µM (PfPMX, PvPMX) or 100-200 µM (PfPMIX) in 1:2-fold dilution for 12 points. The enzyme kinetic assay was allowed to proceed at 37°C for 1 hr in the PHERAstarFSX plate reader (BMG Labtech). Linear slope (0-15 min) was used to determine the initial velocity (RFU/min) and the substrate K_m was calculated in Graphpad Prism based on Michaelis-Menten enzyme kinetics.

For all IC_{50} determination assays, 10-point dilution series of compounds were prepared in 384 well black low volume assay plates (Corning #4514) using an Echo555 (Labcyte). Appropriate volumes of 10 mM compound stocks were transferred into the assay plates with a 1:3-fold dilution series. All wells were backfilled to 200 nl DMSO such that it remained constant across the assay plates (1% final). 10 µl PfPMX or PvPMX (0.05 nM) or PfPMIX (1 nM) enzyme was dispensed into compound containing assay plates. Plates were allowed to incubate for 15 min at room temperature and the reaction was started with a further 10 µl addition of PfRh2N (3.5 µM) for PMX assays or PfRON3 (16.6 µM) for PMIX assay. Plate was incubated at 37°C for 4 hr. Enzyme and substrate solutions were prepared in the above-mentioned assay buffers. Samples were excited at 340 nm and fluorescence emission measured at 480 nm using a PHERAstarFSX plate reader (BMG Labtech). IC_{50} values were calculated by Graphpad Prism software using a nonlinear regression four-parameter fit analysis. The equation used is sigmoidal dose response (variable slope), Y = bottom + (top − bottom)/(1+10((logEC50 − X)×Hill Slope)). Compound K_i values were calculated from the IC_{50}s using the Cheng-Prusoff equation, $Ki = IC_{50}/(1 + [S]/K_m)$.

Peptide cleavage and Mass Spectrometry. PfPMIX and PvPMX cleavage site identification assays were performed as described [3]. Briefly, FRET based peptide subtstrates (listed below) (100 µM) with and without the presence of PvPMX, PfPMX or PfPMIX (50 nM) were incubated in 25 mM ammonium acetate buffer (pH 5.5) at 37°C for 24 hr. The reaction was stopped by filtering the reaction mixture through 10 kDa spin columns (abcam) to remove the protease. The eluant was analyzed on an Agilent LC-ESMS system composed of an Agilent G6120B Mass Detector, 1260 Infinity G1312B Binary pump, 1260 Infinity G1367E HiPALS autosampler and 1260 Infinity G4212B Diode Array Detector MS using an Orbitrap LT Quadrupole mass spectrometer. Conditions for LCMS were as follows, column: Xbridge 300 Å C18, 2.1 × 50 mm 3.5 Micron at 30°C, injection volume of 3 µL. PfRON3 (Dabcyl)-KEISFLERRE(Edans) and PvRON3 (Dabcyl)-NGVSFLQKKE(Edans) were run with a gradient of 3–100% B over 4.5 min, while Rh2N (Dabcyl)-HSFIQEGKEE-(Edans) was run with a gradient of 3-100% B over 6.5 min (solvent A: water 0.1% formic acid; solvent B: AcCN 0.1% formic acid), with a flow rate of 0.6 mL/min and detection at 214 or 224 nm.

Surface Plasmon Resonance. PvPMX or PfPMX proteases were immobilised on a CM5 sensor chip (Cytiva) by amine coupling in 10 mM actetate pH 5.5, injecting for 420 s at a flow rate of 10 mL min^{-1} typically immobilising around 4000 RU of protein. All experiments were performed in HBS-EP buffer (10 mM Hepes pH 7.4, 150 mM NaCl, 3 mM EDTA and 0.05% tween 20) at 18°C with a 30 mL min^{-1} flowrate. The compounds WM4 and WM382 were diluted to appropriate concentrations in the range 0.031 nM to 16 nM in HBS-EP+ buffer. Compounds were injected with a 90 s contact time and 1500 s dissociation,

followed by 30 s regeneration with 50 mM glycine pH 9.5. Experiments were performed independently three times using a freshly immobilised sensor surface. PvPMX data were acquired on a BIAcore S200 instrument with data analysis in Biacore S200 evaluation software version 1.1 (Cytiva) and PfPMX data collected on a BIAcore 8K+ instrument with data analysis in Biacore Insight evaluation software version 3.0.12.15655 (Cytiva). All sensorgrams were double reference using an activated the ethanolamine blocked sensor surface and an HBS-EP+ buffer blank. Affinities were determined using a 1:1 binding model fitting on and off rates for WM4, it was not possible to report affinities for WM382 as the off rate was too slow to determine. Affinities are reported as the mean and one standard deviation for the three independent experiments.

Data Availability

Data Availability

The data that support the findings of this study are available within the paper and its Supplementary Information.

Declarations

Acknowledgements

We thank the Red Cross Blood Service (Melbourne, Australia) for supply of donor blood for our cell culture. This work was possible through support of The Wellcome Trust [109662/Z/15/Z, 202749/Z/16/Z]; Victorian State Government Operational Infrastructure Support and Australian Government NHMRC IRIISS; National Health and Medical Research Council of Australia. This research was undertaken in part using the MX2 beamline at the Australian Synchrotron, part of ANSTO, and made use of the Australian Cancer Research Foundation (ACRF) detector. We acknowledge the CSIRO Collaborative Crystallisation Centre (www.csiro.au/C3), Melbourne, Australia for screening conditions for crystallisation of PfPMX and PfPMX/inhibitor complexes.

Author contributions

ANH and JC conceived and performed experiments, analyzed data, and wrote the manuscript. SS, JC, ANH, MD collected X-ray data, solved and built structures. TT made HA-tagged parasites and identified new substrates of PfPMIX. AN, KL performed peptide cleavage assays and enzyme kinetic analyses. PF conceived experiments and responsible for project management. RB and PC performed and analysed SPR. WHT was involved in structural determination of PfPMX. NM gathered and aligned sequences. BB and BS performed Mass Spectrometry experiments. ZG performed the homology modelling with PfPMIX. DO, PF, MR, JM conceived experiments and analysed small molecule/protein data. AFC conceived experiments, analysed data, and wrote the manuscript.

Competing interests

MR, PF, ZG, JM, BS, TT, DO and AFC have a patent Antimalarial Agents PCT/CN2019/100781 based on compounds in this manuscript. MR, DO, ZG, NM and JM are employees of Merck Sharp & Dohme Corp., a subsidiary of Merck & Co., Inc., Kenilworth, NJ, USA and may own stock or hold stock options in Merck & Co., Inc., Kenilworth, NJ, USA.

References

1. Nasamu AS, *et al.* Plasmepsins IX and X are essential and druggable mediators of malaria parasite egress and invasion. *Science* **358**, 518–522 (2017).
2. Pino P, *et al.* A multistage antimalarial targets the plasmepsins IX and X essential for invasion and egress. *Science* **358**, 522–528 (2017).
3. Favuzza P, *et al.* Dual Plasmepsin-Targeting Antimalarial Agents Disrupt Multiple Stages of the Malaria Parasite Life Cycle. *Cell Host Microbe* **27**, 642-658 e612 (2020).
4. Cowman AF, Healer J, Marapana D, Marsh K. Malaria: Biology and Disease. *Cell* **167**, 610–624 (2016).
5. Giovannini D, *et al.* Independent roles of apical membrane antigen 1 and rhoptry neck proteins during host cell invasion by apicomplexa. *Cell Host Microbe* **10**, 591–602 (2011).
6. Yap A, *et al.* Conditional expression of apical membrane antigen 1 in *Plasmodium falciparum* shows it is required for erythrocyte invasion by merozoites. *Cell Microbiol* **16**, 642–656 (2014).
7. Duraisingh M, *et al.* Phenotypic variation of Plasmodium falciparum merozoite proteins directs receptor targeting for invasion of human erythrocytes. *Embo Journal* **22**, 1047–1057 (2003).
8. Sahar T, *et al. Plasmodium falciparum* Reticulocyte Binding-Like Homologue Protein 2 (PfRH2) Is a Key Adhesive Molecule Involved in Erythrocyte Invasion. *PLoS One* **6**, e17102 (2011).
9. Weiss GE, *et al.* Revealing the Sequence and Resulting Cellular Morphology of Receptor-Ligand Interactions during *Plasmodium falciparum* Invasion of Erythrocytes. *PLoS Pathog* **11**, e1004670 (2015).
10. Wong W, *et al.* Structure of *Plasmodium falciparum* Rh5-CyRPA-Ripr invasion complex. *Nature* **565**, 118–121 (2019).
11. Proellocks NI, *et al.* Characterisation of PfRON6, a *Plasmodium falciparum* rhoptry neck protein with a novel cysteine-rich domain. *Int J Parasitol* **39**, 683–692 (2009).
12. Sherling ES, *et al.* The *Plasmodium falciparum* rhoptry bulb protein RAMA plays an essential role in rhoptry neck morphogenesis and host red blood cell invasion. *PLoS Pathog* **15**, e1008049 (2019).
13. Low LM, *et al.* Deletion of *Plasmodium falciparum* Protein RON3 Affects the Functional Translocation of Exported Proteins and Glucose Uptake. *mBio* **10**, (2019).
14. Haase S, *et al.* Characterization of a conserved rhoptry-associated leucine zipper-like protein in the malaria parasite *Plasmodium falciparum*. *Infection and Immunity* **76**, 879–887 (2008).
15. McCartney CE, Davies PL. FRET-Based Assays to Determine Calpain Activity. *Methods Mol Biol* 1915, 39-55 (2019).

16. O'Keeffe AH, Green JL, Grainger M, Holder AA. A novel Sushi domain-containing protein of *Plasmodium falciparum*. *Mol Biochem Parasitol* **140**, 61–68 (2005).
17. Chen L, *et al.* An EGF-like protein forms a complex with PfRh5 and is required for invasion of human erythrocytes by *Plasmodium falciparum*. *PLoS Pathog* **7**, e1002199 (2011).
18. Navia MA, *et al.* Three-dimensional structure of aspartyl protease from human immunodeficiency virus HIV-1. *Nature* **337**, 615–620 (1989).
19. Hodder AN, *et al.* Structural basis for plasmepsin V inhibition that blocks export of malaria proteins to human erythrocytes. *Nat Struct Mol Biol* **22**, 590–596 (2015).
20. Khan AR, James MN. Molecular mechanisms for the conversion of zymogens to active proteolytic enzymes. *Protein Sci* **7**, 815–836 (1998).
21. Trager W, Jensen JB. Human malaria parasites in continuous culture. *Science* **193**, 673–675 (1976).
22. Jain NK, *et al.* A high density CHO-S transient transfection system: Comparison of ExpiCHO and Expi293. *Protein Expr Purif* **134**, 38–46 (2017).
23. Panjikar S, Parthasarathy V, Lamzin VS, Weiss MS, Tucker PA. Auto-rickshaw: an automated crystal structure determination platform as an efficient tool for the validation of an X-ray diffraction experiment. *Acta Crystallogr D Biol Crystallogr* **61**, 449–457 (2005).
24. Emsley P, Cowtan K. Coot: model-building tools for molecular graphics. *Acta Cryst D Biol Crystallogr* **60**, 2126–2132 (2004).
25. Liebschner D, *et al.* Macromolecular structure determination using X-rays, neutrons and electrons: recent developments in Phenix. *Acta Crystallogr D Struct Biol* **75**, 861–877 (2019).
26. Kabsch W. XDS. *Acta crystallographica Section D, Biological crystallography* **66**, 125–132 (2010).
27. Evans PR. An introduction to data reduction: space-group determination, scaling and intensity statistics. *Acta Crystallogr D Biol Crystallogr* **67**, 282–292 (2011).
28. Evans PR, Murshudov GN. How good are my data and what is the resolution? *Acta Crystallogr D Biol Crystallogr* **69**, 1204–1214 (2013).
29. Adams PD, *et al.* PHENIX: a comprehensive Python-based system for macromolecular structure solution. *Acta Cryst D Biol Crystallogr* **66**, 213–221 (2010).
30. Jurrus E, *et al.* Improvements to the APBS biomolecular solvation software suite. *Protein Sci* **27**, 112–128 (2018).

Figures

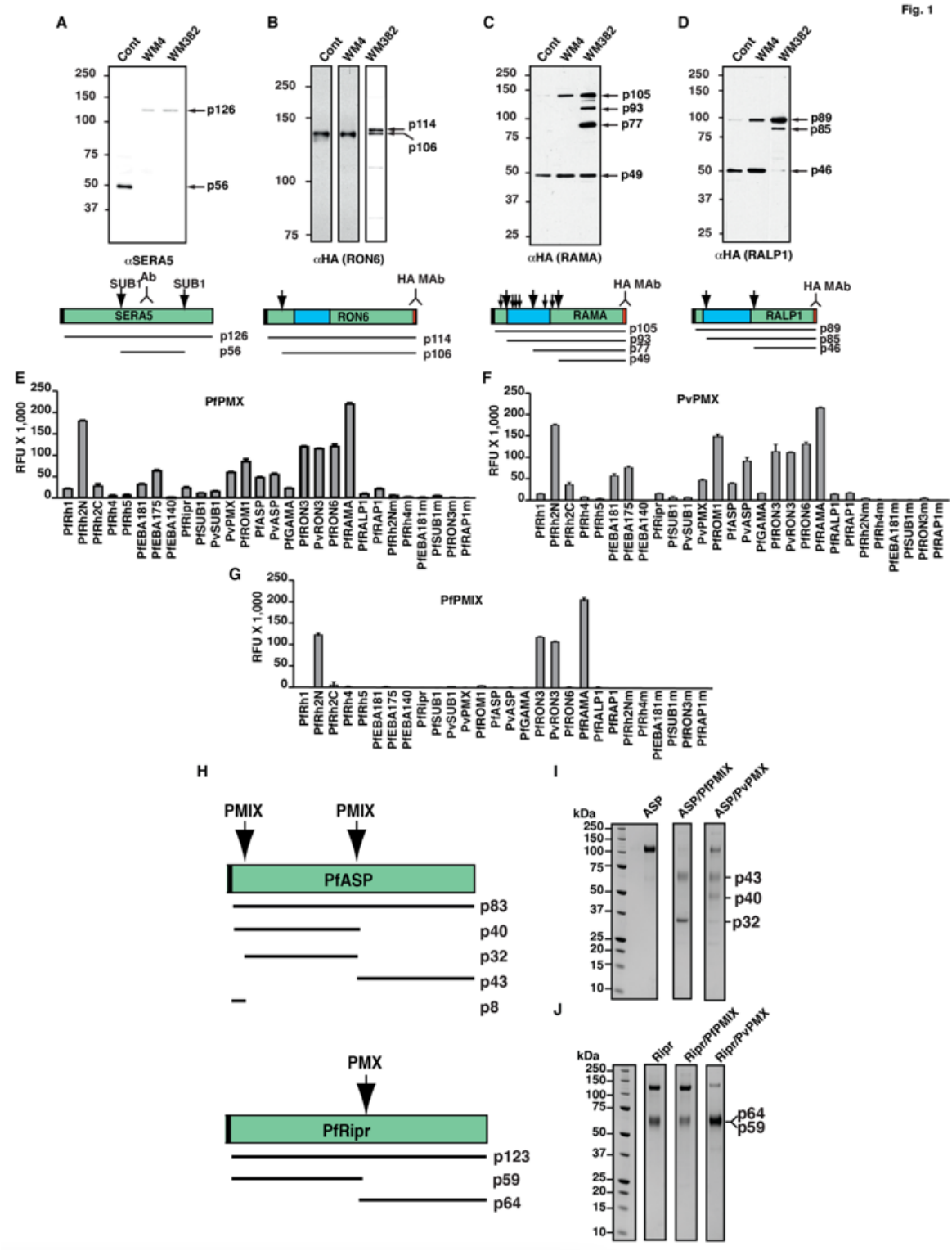

Figure 1

PMIX is responsible for processing P. falciparum proteins and can be inhibited by WM382 but not WM4. A. SERA5 processing was blocked by WM4 and WM382. Shown are supernatants containing proteins released from merozoites. SERA5 was detected using a specific antibody as shown by the Ab symbol. Shown are parasites: not treated (Cont), WM4-treated or WM382-treated. B. RON6 is processed by PMIX. RON6 was tagged with HA epitopes at the C-terminus and detected using anti-HA antibodies. Shown are

parasites: not treated (Cont), WM4-treated or WM382-treated. Blue domain shows a repetitive amino acid region. C. RAMA is processed by PMIX. RAMA was tagged with HA epitopes at the C-terminus and detected using anti-HA antibodies. Shown are parasites: not treated (Cont), WM4-treated or WM382-treated. RALP1 was tagged with HA epitopes at the C-terminus and detected using anti-HA antibodies. Shown are parasites: not treated (Cont), WM4-treated or WM382-treated. For panels B-D, proteins of interest were detected using 3D7 parasites in which they had been tagged with a HA-epitope at the C-terminus (shown as red box) and detected with anti-HA antibodies. The position of the detecting antibody for each immunoblot is signified by the Ab symbol. The black domain at the N-terminus corresponds to the signal sequence and the blue domain signifies a repetitive amino acid region. D. RALP1 was processed by PMIX. Molecular weight markers are shown in kDa at the left of each panel. E-G. Cleavage of fluorogenic peptides corresponding to processing sites from P. falciparum and P. vivax proteins by recombinant plasmepsin proteases. Each histogram represents three independent experiments with standard deviation. E. PfPMX, F. PvPMX, G. PfPMIX. H. Position of PMIX and PMX cleavage sites for PfASP and PfRipr. Calculated molecular weights are shown below with the position of each processed polypeptide indicated by the corresponding line. I. Processing of PfASP by PvPMX and PfPMIX visualized using Coomassie staining. Molecular weight markers are shown on the left in kDa. K. Processing of PfRipr by PfPMIX and PvPMX visualized using Coomassie staining. Molecular weight markers are shown on the left in kDa.

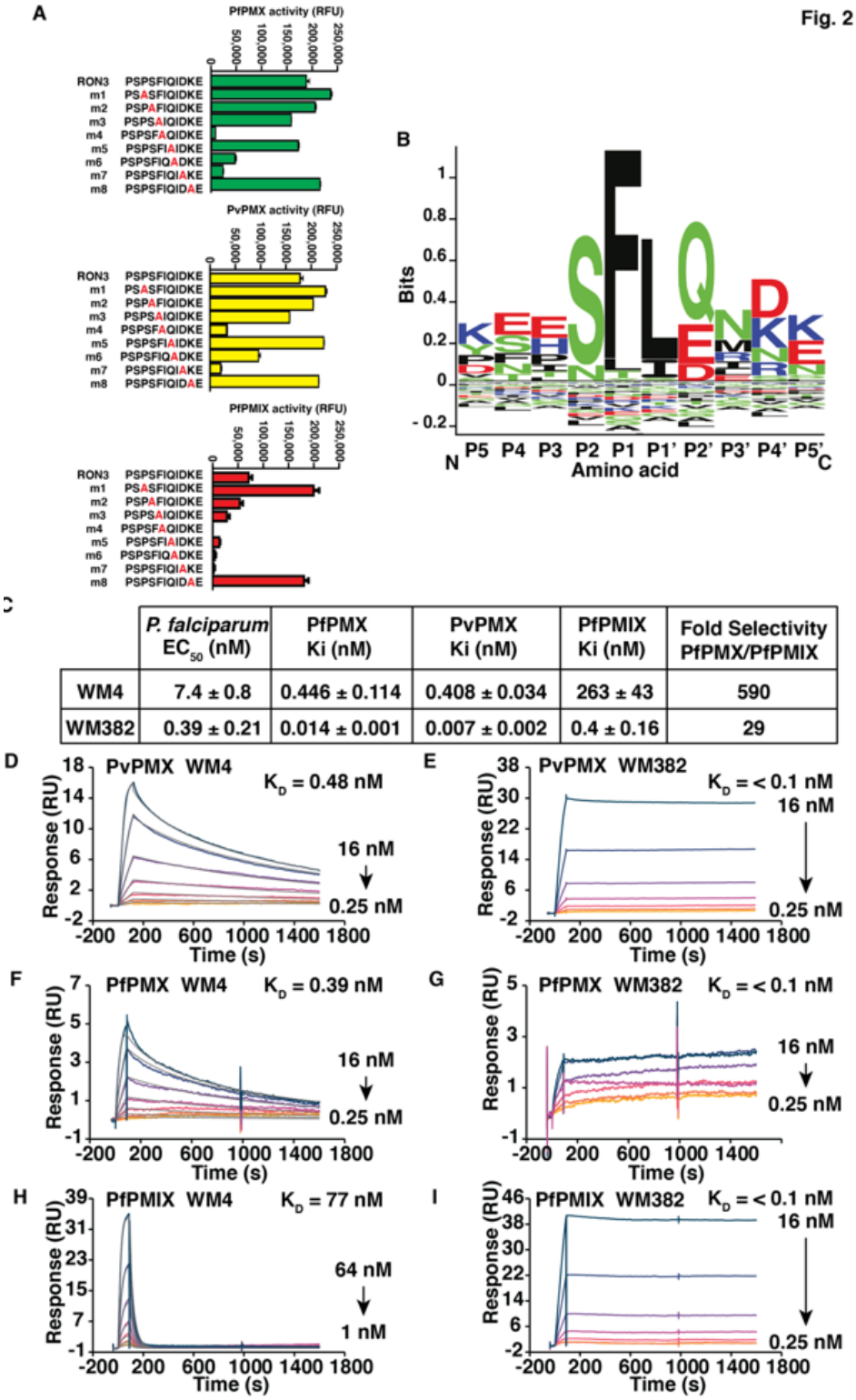

C

	P. falciparum EC_{50} (nM)	PfPMX Ki (nM)	PvPMX Ki (nM)	PfPMIX Ki (nM)	Fold Selectivity PfPMX/PfPMIX
WM4	7.4 ± 0.8	0.446 ± 0.114	0.408 ± 0.034	263 ± 43	590
WM382	0.39 ± 0.21	0.014 ± 0.001	0.007 ± 0.002	0.4 ± 0.16	29

Figure 2

PfPMX, PVPMX and PfPMIX have similar substrate specificity and are differentially inhibited by WM4 and WM382. A. Cleavage of fluorogenic RON3 peptides corresponding to the processing site from P. falciparum by recombinant PfPMIX (red), PfPMX (green) and PvPMX (yellow). Each histogram represents three independent experiments with standard deviation. B. Sequence logo representation of the occurrence of amino acids residues in the cleavage site P5-P5' positions of PMIX substrates (Schneider

and Stephens, 1990). C. Determination of Ki for WM4 and WM382 for PfPMX, PvPMX and PfPMIX and fold selectivity (PfPMX Ki/PfPMIX Ki). Also shown are EC50 values for inhibition of P. falciparum growth. Data represents mean and Standard Deviation for at least three independent experiments. D-I. Representative sensograms from the surface plasmon resonance (SPR) based binding assays for the interaction of PvPMX (D and E), PfPMX (F and G) and PfPMIX (H and I) recombinant protease with WM4 and WM382. Each graph represents an independent experiment showing titrations of each compound from 16 nM (Blue) to 0.25 nM (orange) in coloured lines. Calculated fits for WM4 binding are shown with grey lines, it was not possible to determine fits to WM382 as the dissociation was too slow. Kinetic parameters for WM4 are shown in Table S1. Experiments D-E were performed independently three times using a freshly immobilised sensor surface. Affinities are reported as the mean and one standard deviation for the three independent experiments.

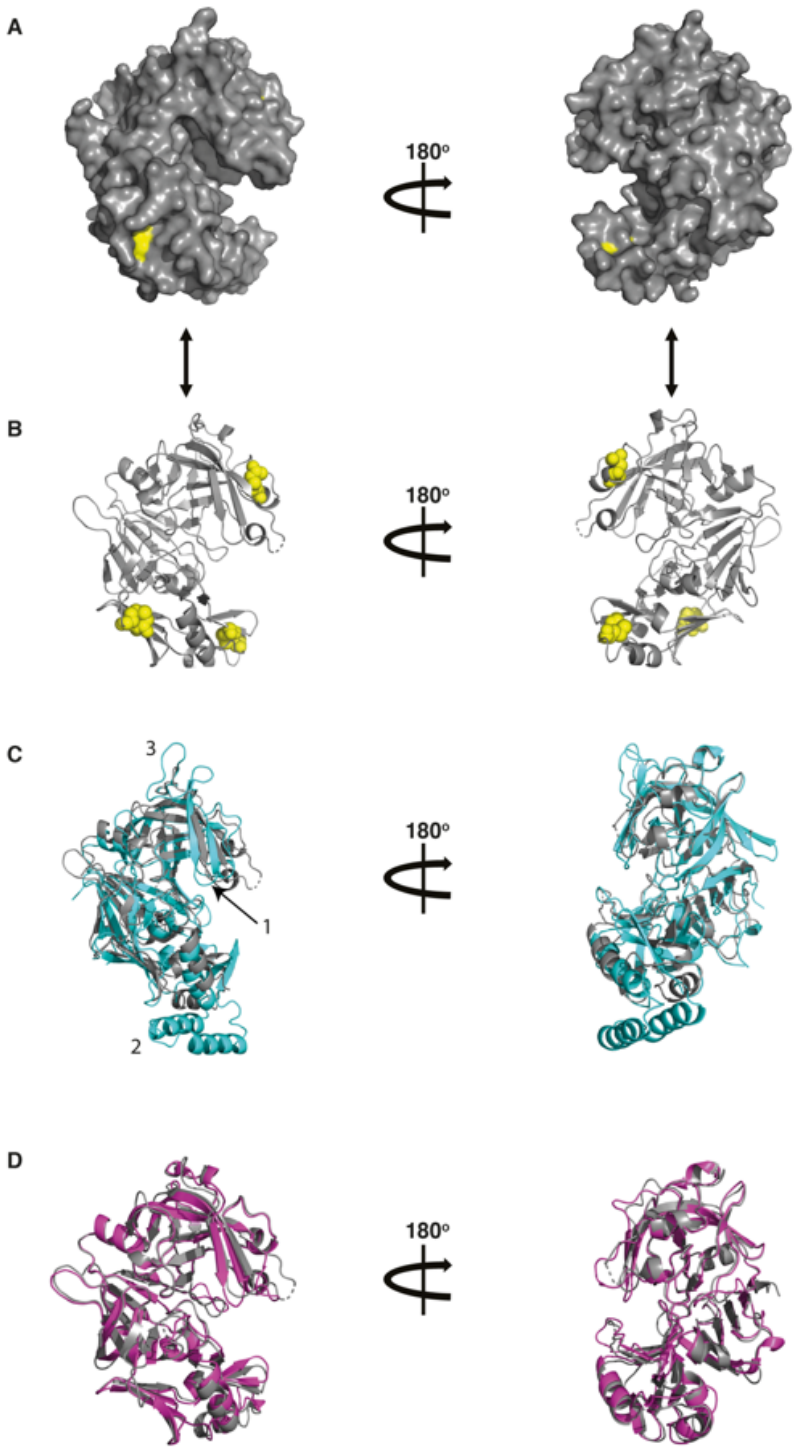

Figure 3

Figure 3

Structure and features of the enzyme domain for PfPMX aspartic protease. A. Schematics showing the structure of P. falciparum PMX apoenzyme. Shown are side to side views (180˚ rotation) in surface representation. The Cys residues (spheres) that form disulphide bonds are shown in yellow. B. Corresponding ribbon diagrams are shown in the equivalent orientations. The disulfide bonded Cys residues (spheres) are shown in yellow for both A and B. C. Comparison of the structures for PfPMX

(grey) and PvPMV (cyan:PDB accession code 4ZL4, without inhibitor for simplicity) shown in ribbon diagrams. RMSD=2.358 (198 to 198 residues) for the Cα chain of each structure, ie; K44-P470 for PvPMV and E234-K570 for PfPMX apo. The loop positioned at the front of the substrate binding cleft for PfPMX (grey) and PvPMV (cyan) are labelled in the diagram as 1 and indicated with an arrow. The two β-barrels present at the bottom of the PvPMV structure are labelled as 2 and the NAP1 fold at the top of the PvPMV structure is labelled as 3. D. Comparison of the PfPMX (grey) structure overlaid on the model structure of PfPMIX (magenta).

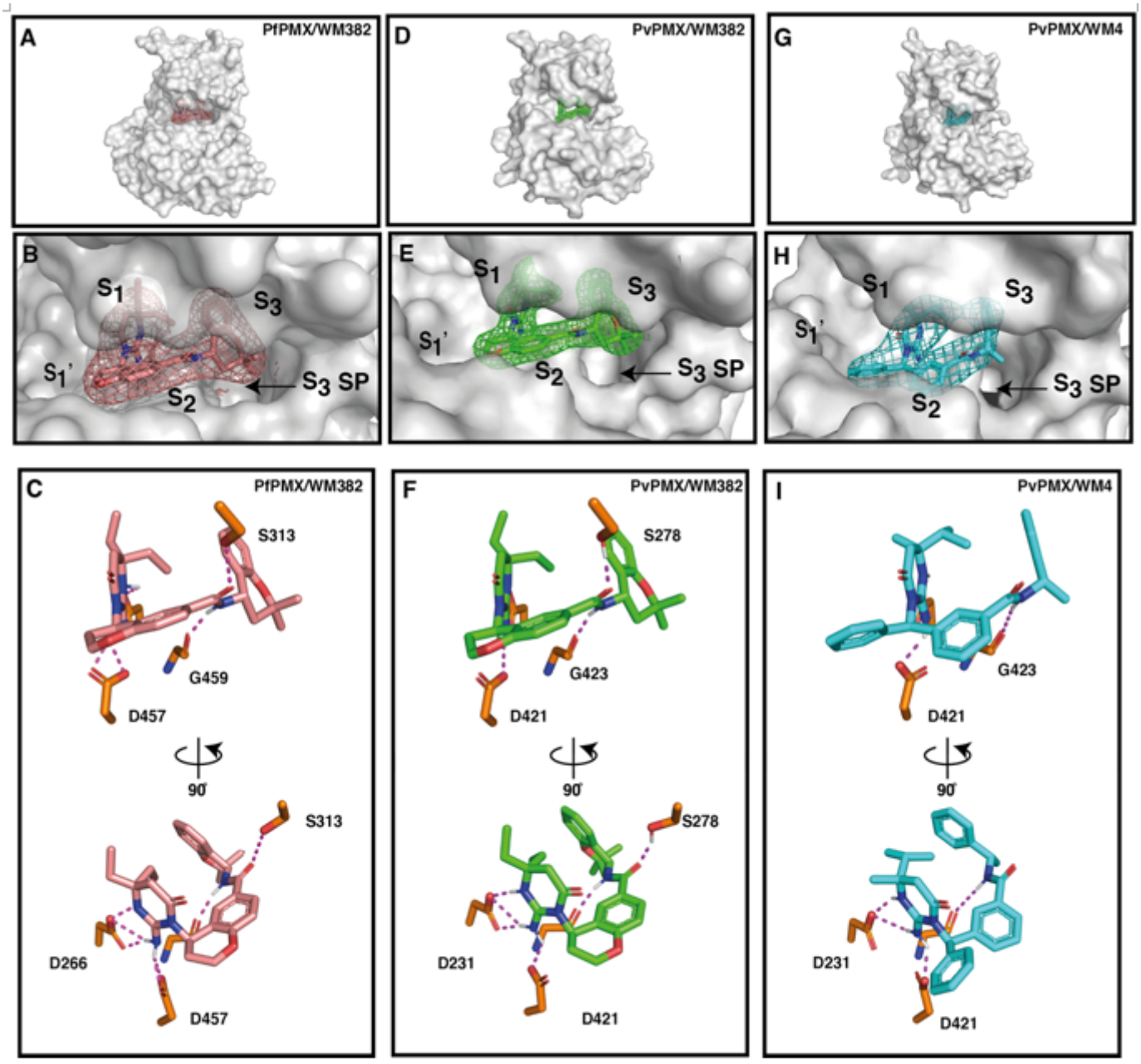

Figure 4

Figure 4

Structures of PfPMX and PvPMX in complex with WM382 and WM4. A. Electron density map (OMIT) of WM384 (pink) located within the active site of PfPMX (Grey) shown as an entire molecule view. B.

Electron density map (OMIT) of WM384 (pink) located in the active site of PfPMX (Grey) magnified view. Position of the defined substrate binding pockets (S) of the active site are shown. 2Fo-Fc density contoured at 1.0 σ. C. Front and side view of a stick structure diagram showing hydrogen bond interactions between WM382 (pink) and the relevant active site residues of PfPMX (orange). D. Electron density map (OMIT) of WM384 (green) located within the active site of PvPMX (Grey) shown as an entire molecule view. E. Electron density map (OMIT) of WM384 (green) located in the active site of PvPMX (Grey) shown as a magnified view. Position of the defined substrate binding pockets (S) of the active site are shown. F. Front and side view of a stick structure diagram showing interactions between WM382 (green) and the relevant active site residues of PvPMX (orange). G. Electron density map (OMIT) of WM4 (blue) located within the active site of PvPMX (Grey) shown as an entire molecule view. H. Electron density map (OMIT) of WM4 (blue) located in the active site of PvPMX (Grey) shown as a magnified view. Position of the defined substrate binding pockets (S) of the active site are shown. I. Front and side view of a stick structure diagram showing interactions between WM4 (blue) and the relative active site residues of PvPMX (orange).

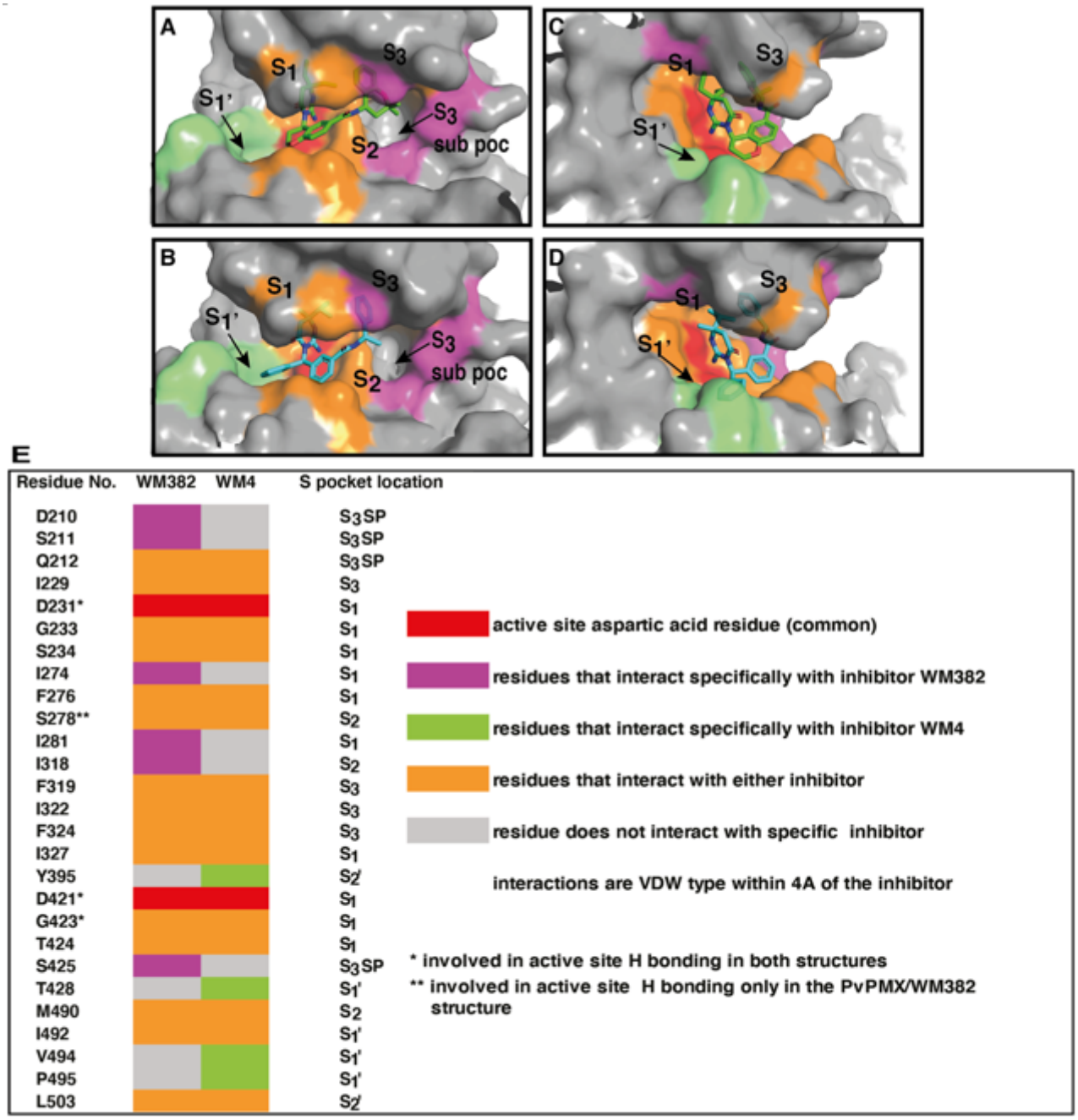

Figure 5

Figure 5

Surface interactions occurring at the interface of the inhibitor – substrate binding cleft. A and C. PvPMV/WM382 and B. and D. PvPMX/WM4 highlight the distribution of common and specific inhibitor interactions within the substrate binding cleft. Although interacting with both inhibitors, the active site aspartic acid residues are shown in red to assist with orientation. WM382 is represented as a green organic compound while WM4 is coloured cyan. Left-hand side view is from the front of the substrate binding cleft (Fig. 5A and B). The RHS view (fig. 5C and D) is from a 900 anti-clockwise rotation about the vertical axis to give a side view into the substrate binding cleft. E. Table comparing the VDW surface interactions (<4 Å) occurring between PvPMX and inhibitors WM382 and WM4. The substrate pocket (S)

location of each residue is shown on the right-hand side. Residues have been colour coded as shown in the Table key. * or ** indicates a residue is involved in hydrogen bonding with an inhibitor(s). The location of each residue has been transposed onto surface representations of the structures for PvPMX /WM382 complex (Fig. 5 A and C) and PvPMX/WM4 complex (Fig. 5 B and D).

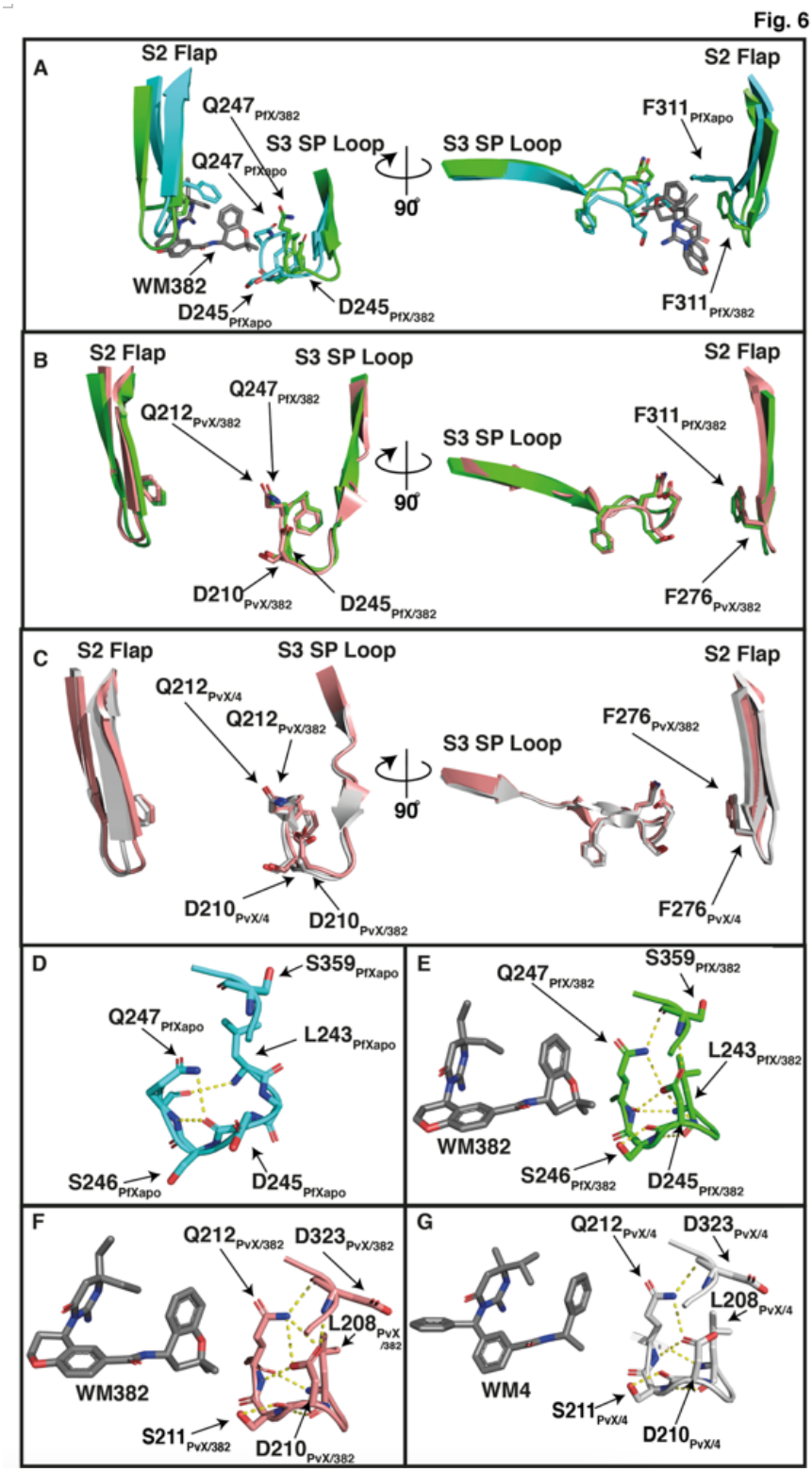

Figure 6

Inhibitor-induced changes to the structure of the PMX substrate binding cleft. A. Schematic representation of the overlaid structures for PfPMX apo (cyan) and the PfPMX/WM382 (green) complex S2 flap and S3SP loop showing the comparative changes in orientation and positioning of residues influenced by the binding of WM382. LHS view is from the front of the substrate binding cleft while the RHS view is from a 900 anti-clockwise rotation about the vertical axis. B. Schematic representation of the overlaid structures for PfPMX/WM382 (green) and PvPMX/WM382 (pink) complexes S2 flap and S3SP loop. Views as per (A). C. Schematic representation of the overlaid structures for PvPMX/WM382 (pink) and PvPMX/WM4 complexes (light grey) S2 flap and S3SP loop. Views as per (A). D. Schematic showing the hydrogen bonds involving residues (L243 to Q247) within the S3SP loop for the PfPMX apo structure. Refer to Table S3 for details of connectivities. E. Schematic showing the hydrogen bonds involving residues (L243 to Q247) within the S3SP loop for the PfPMX-WM382 structure refer to Table S3 for details of the connectivities. F. Schematic showing the hydrogen bonds involving residues (L208 to Q212) within the S3SP loop for the PvPMX/WM382 structure (Table S3). G. Schematic showing the hydrogen bonds involving residues (L208 to Q212) within the S3SP loop for the PvPMX/WM4 structure refer to Table S3 for details of connectivity.

Supplementary Files

This is a list of supplementary files associated with this preprint. Click to download.

- SupplementaryFiguresandTables.docx